J Nanopart Res (2020) 22: 94
https://doi.org/10.1007/s11051-020-04825-7

RESEARCH PAPER

Nanosize inclusions as a fingerprint for aeolian sediments

Ali Al-Dousari · Ken Pye · Abdsalam Al-Hazza · Fatima Al-Shatti · Modi Ahmed · Noor Al-Dousari · Mohamad Rajab

Received: 2 March 2020 / Accepted: 24 March 2020 / Published online: 18 April 2020

Abstract Backscattered electron microscopy was used to analyze the inclusions within twelve different samples from dunes (Recent) and the Dibdiba Formation (Miocene to Pleistocene) sediments. The twelve aeolian samples were collected from a line transect across the main wind corridor, representing the downwind, mid, and upwind areas (three in each set). All examined samples are noted in the major elements within minerals. The most dominant elements detected elements within aeolian samples are iron, aluminum, calcium, and zirconium, respectively. On the other hand, some differences were observed. Generally, lower inclusion counts were noted within quartz and feldspars in the downwind samples in comparison with other samples. The aluminum percentages gradually increase upwind. The mid-area samples show more sodium compared with up and downwind. The average percentages of detected barium within inclusions in quartz and feldspar particles show gradual increases downwind. The Dibdiba Formation samples show uniformity between major elements in all samples. The variations between samples are very limited. Titanium, for example, through natural solubility in smectite is concentrated in cracks, fractures, or borders of quartz particles to form rutile (TiO_2) with needle-like or lath-like crystals. The military tanks and missiles that were used in Kuwait Liberation War (1990–1991) are believed to be the main source of titanium that forms inside particle cavities, cracks, and borders. Furthermore, no further changes were noticed during the comparison between the barium inclusions within quartz that are found in both the Dibdiba Formation (4.7%) and the aeolian (4.8%) samples. Other elements show nearly the same trend of similarities during the comparison between samples.

Keywords Aeolian · Nanosize · Inclusions · Elements · Electron microscope · Kuwait

This article is part of the Topical collection on *Nanotechnology in Arab Countries*

A. Al-Dousari (✉) · A. Al-Hazza · F. Al-Shatti · M. Ahmed · N. Al-Dousari
Kuwait Institute for Scientific Research (KISR,) Environment and Life Sciences Research Center, Kuwait City, Kuwait
e-mail: adousari@kisr.edu.kw

K. Pye
Geology Department, Royal Holloway University of London (RHUL), Egham, UK

M. Rajab
Nonoscopy Science Center, Kuwait University (KU), Kuwait City, Kuwait

Introduction

The analysis of polished sections of rocks and particle mounts using the backscattered scanning electron microscope (BSE) mode has assumed particular importance in the mineral sciences owing to the need to acquire large amounts of quantitative mineralogical information together with morphological data (Krinsley et al. 1998; Vignesh et al. 2013; Malathy et al. 2014). The backscattered electron microscopy (BSE) images can be useful in studying the loose sediment particles

(Sudha et al. 2012). BSE images utilize the variances in the gray-scale brightness of diverse mineral phases. BSE image (average atomic number differences) can be useful in studies that aim to quantify the relative degrees of weathering of different minerals within loose sediments or natural rock samples and can provide important information from particle inclusions. Chalcraft and Pye (1984) used BSE to identify the weathering features on natural outcrops of Precambrian quartzite at Mount Roraima in southeastern Venezuela. They found that the breakdown of the rock initiated primarily as a result of silica solution along quartz particle boundaries. Spaces between particles progressively widen due to solution and allow better penetration of meteoric fluids into the quartzite, which enhances the rate of weathering through the process of feedback. Any remaining feldspar in the rock is rapidly altered to kaolinite, some of which is redistributed along the particle-boundary cracks (Krinsley et al. 1998). Using the relative peak intensities in the identification of minerals is used for a limited group of minerals. Peak intensities are somewhat dependent on instrumental factors, including accelerating voltage. Moreover, many minerals exhibit a considerable range of composition (Reed and Ware 1975). Some minerals identification was done via correlation between the identified heavy and light minerals done in previous analysis and the ED (energy-dispersive) spectra of common minerals given by Reed and Ware (1975). The backscattered microscope analysis of inclusions within quartz and feldspar particles of aeolian sand is not widely used (Aba et al. 2016; Al-Dousari et al. 2016). The quartz and feldspars represent more than 90% of the aeolian dune sediments in Arabia, including Kuwait (Al-Awadhi et al. 2000; Abd El-Wahab et al. 2018). Therefore, the aim of this study is to detect special variations of dune sediments in terms of their inclusions content and compare it with surrounding sediments in the Dibdiba Formation (Miocene to Pleistocene).

Methodology

Samples were collected to represent a transect along the wind corridor from upwind to downwind and included three different sets of aeolian samples within the main wind corridor and one extra set from the Dibdiba Formation for comparison (Fig. 1). These samples were carefully impregnated with epoxy, cut, and polished. The first set of three aeolian samples was from the far upwind area around the Huwamiliyah area. These samples are upwind. The second set of aeolian samples is located downwind in the Atraf area, while samples of mid-area are from areas in between. The Dibdiba Formation is represented by one set of three samples and were picked from the fine sand size particles (0.250–0.180 mm), while all the rest of the aeolian samples or sediments are from the medium sand fractions (0.5–0.350 mm) as it represents the most dominant of the dominant size fractions. Sample from both size fractions was split, mixed, and placed on a resin block to allow the preparation of a polished surface. Procedures for grinding and polishing of aeolian sediment samples include the use of several grades of diamond abrasive.

A Hitachi 3000 variable pressure SEM equipped with BSE deflectors was used to analyze the samples. The microscope can be used in several modes to:

(a) Image the sample in BSE or SEM mode.
(b) Spot analysis, areas, or line cross sections using the EDX attachment.
(c) Map element distributions.

The main elements within detected inclusions in quartz, feldspar, and other particles were studied carefully. The identification of some mineral species is difficult since there are some minerals that are polymorphs that have the same chemical composition but a different structure. For example, there are seven known polymorphs of TiO_2 that have the same chemical composition (e.g., rutile, anatase, and brookite) but with different structures. As a result, identification is done mainly through the form of crystals where rutile (TiO_2) may take the form of long hair-like needles while others are either euhedral lath-like or other forms.

Results and discussion

Analysis of the BSE images showed that quartz is the dominant mineral in all samples. K-feldspar, plagioclase, clay, and calcrete occur in appreciable amounts with few heavy minerals. The variation between samples in both aeolian and Dibdiba Formation in mineralogy is rare. However, some exotic and rare elements appear in the composition of some inclusions in specific samples and not in others.

Six main elements were detected within the inclusions: titanium (Ti), zirconium (Zr), iron (Fe), calcium (Ca),

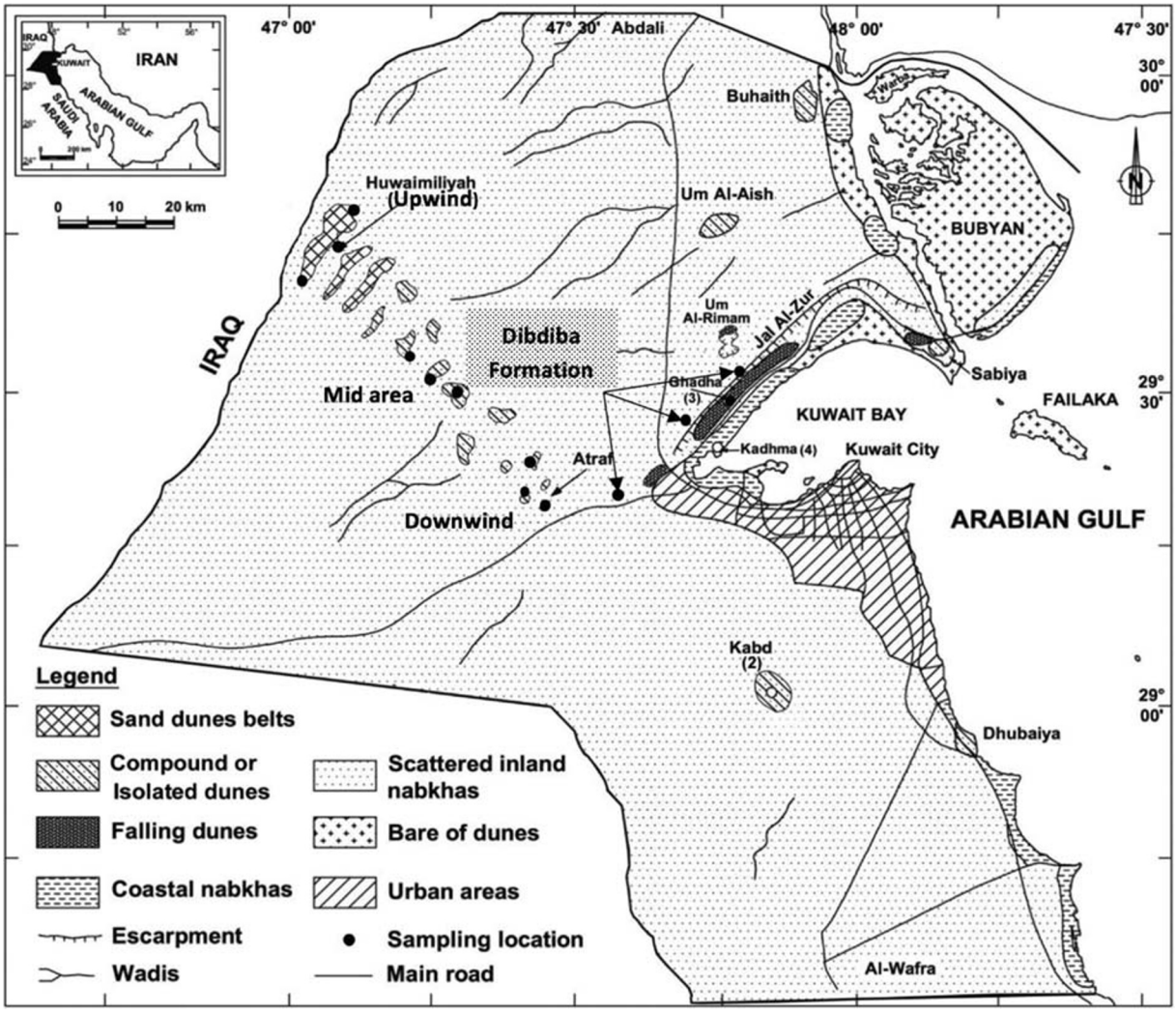

Fig. 1 The sample locations from upwind, mid-area, and downwind sand dunes and the Dibdiba Formation

aluminum (Al), and molybdenum (Mo). Barium (Ba), potassium (K), magnesium (Mg), sodium (Na), and manganese (Mn) were also found in appreciable amounts.

Major particle characteristics

Three major particle types have been classified according to mineralogy. These are quartz, feldspars, and other particles. The particle characteristics are discussed in this paper in terms of shape, alteration products, inclusion types, distribution, and interrelationships between Dibdiba Formation and aeolian samples.

The mineralogical characteristics of aeolian samples are mostly similar. The downwind samples are dominantly composed of quartz (91.5%) with very little feldspar (6%). The K-feldspar (3.7%) appears usually but not always free of any inclusions (Fig. 2a). The mid samples are composed of 94% of quartz, 3.6% carbonates, and 2.4% percentage for feldspars (Fig. 2b and c). The quartz represents 93.1% of the total particles within the sample (Fig. 2d and e), while K-feldspar and clay represent 2.7% and 4.1%, respectively, in upwind samples. Although the percentage of K-feldspar is a little high (12.2%) in upwind samples compared with other samples, it contains very little inclusions within feldspar particles. The quartz particles represent 85.4% and clay particles represent 2.4% (Fig. 2f). This mineral constitutes are common in aeolian dust in the region but with lesser percentages (Al Enezi et al. 2014; Aba et al. 2018; Al-Dousari et al. 2019a).

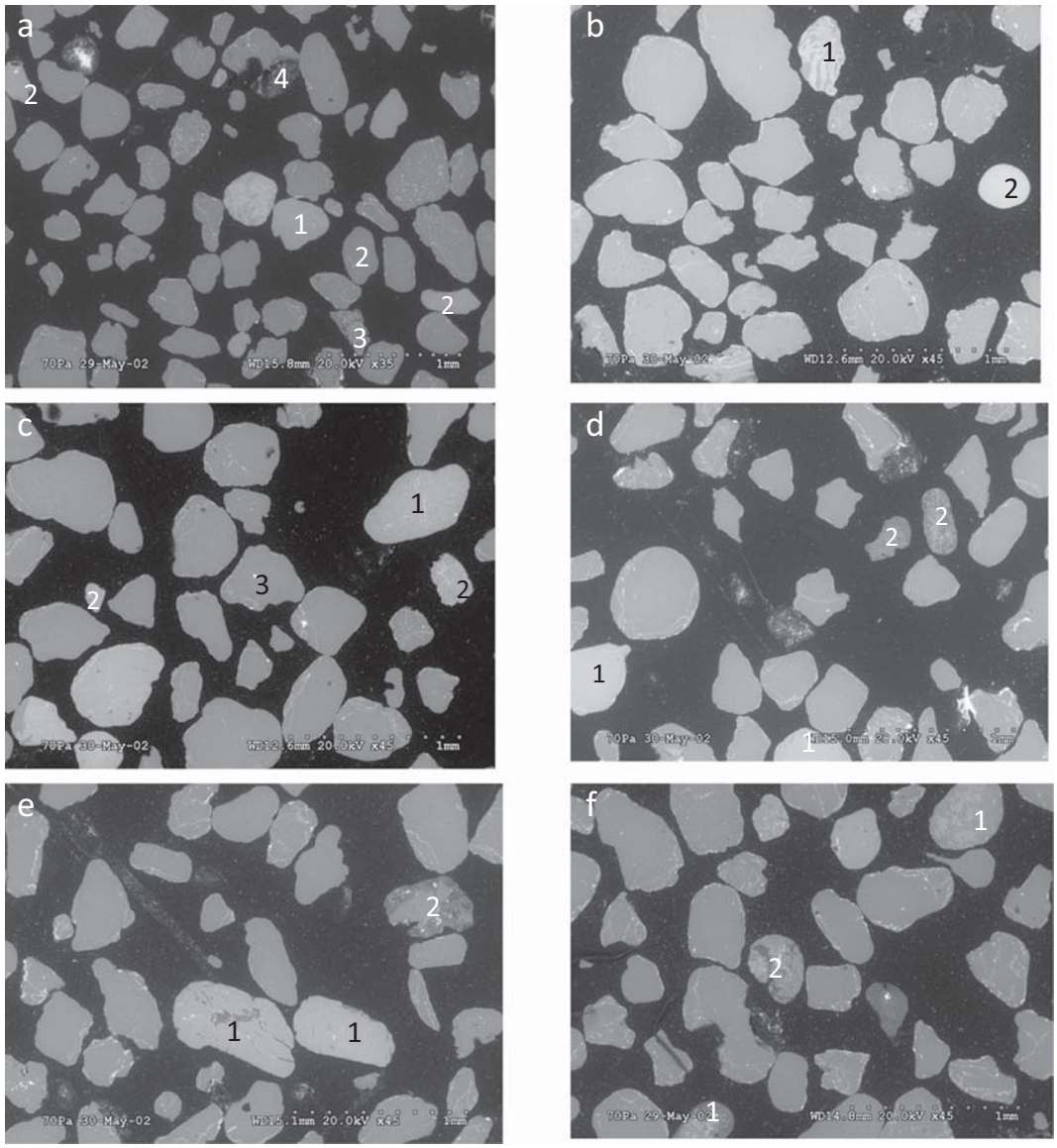

Fig. 2 Aeolian samples represented by **a** samples of downwind is dominantly composed of well-rounded corners of quartz particles with minor K-feldspar (1), plagioclase (2), mud particles (calcrete and mud pellets), (3) and heavy minerals (4); **b** samples of upwind where the quartz is dominant with few perthite particles (1) and well-rounded carbonate particle (calcite) (2); **c** another view of samples upwind showing K-feldspar particles characterized by brightness variation (1), angular particles of carbonate and quartz particles containing zircon inclusions (3); **d** upwind sample containing two particles of plagioclase (1) and two other particles of dissolved K-feldspar affected by diagenesis in an early stage of forming clay minerals (2); **e** another view of the upwind sample showing two K-feldspars (1) surrounded by quartz particles with one single particle of mud containing quartz fractions (2); **f** K-feldspar particles (1) in the upwind sample with a single mud pellet (2)

The quartz represents 89.9% of the average total particles in all tested samples. As a result, most of the detected inclusions were found within quartz particles. Although the majority of quartz particles contain no inclusions, many quartz particles with inclusions, cavities, and features were observed (Fig. 3a). Some inclusions were observed as isolated crystals inside the quartz particles, and appear to have formed during the early stages of crystallization. Other inclusions were formed due to diagenesis within cavities, fractures, or borders of the particles and associated dominantly with clay minerals, especially smectite. The former type of

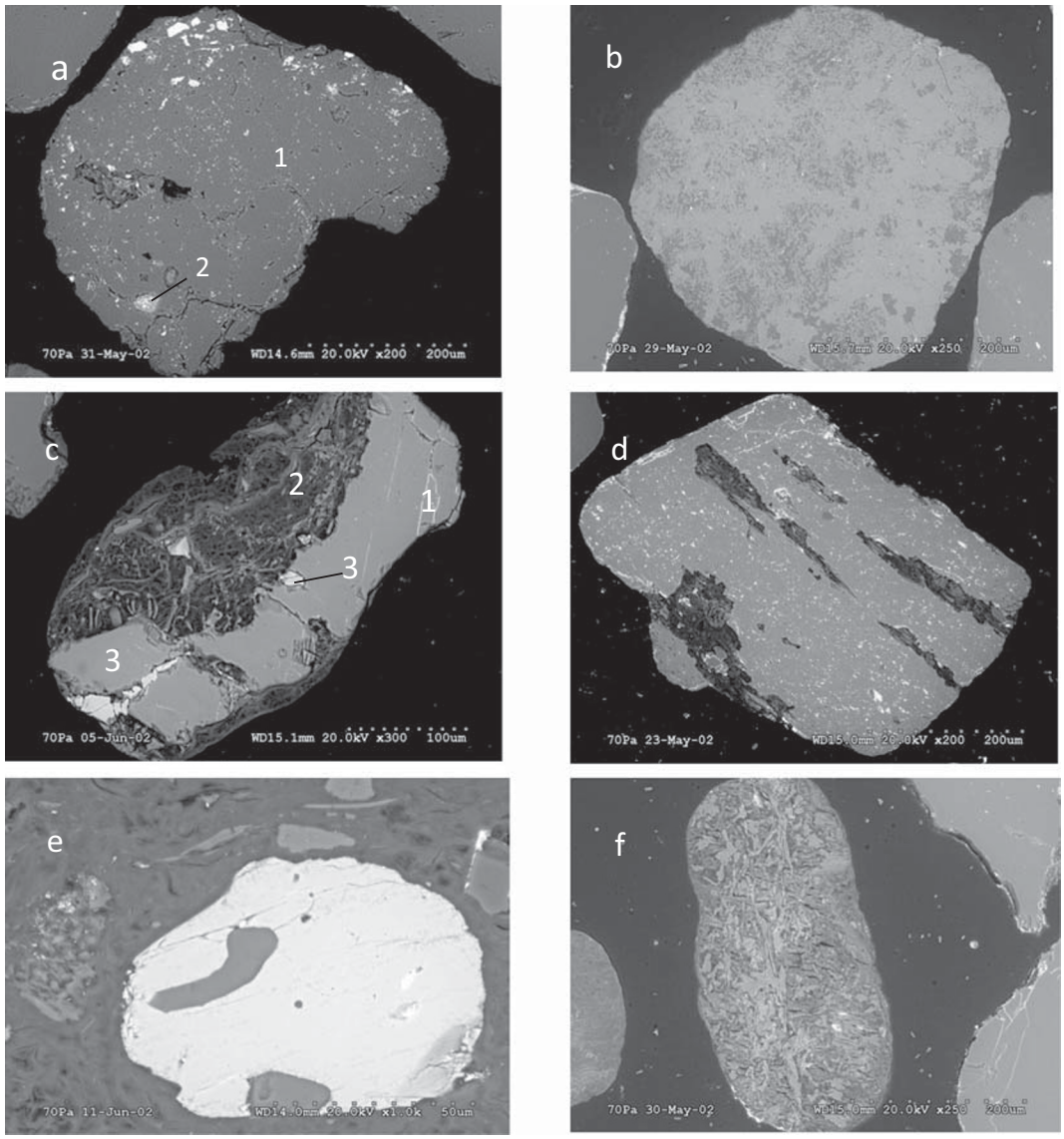

Fig. 3 Characteristics of major particle types: **a** a quartz particle full of inclusions of (1) zircon and heavy minerals composed of silica and titanium with lesser iron, zirconium, and aluminum; **b** a well-rounded K-feldspar particle that is free of any inclusions showing brightness variation due to variation in potassium concentration; **c** intergrowth of (1) K-feldspar with (2) pyroxene, and (3) a vein of mineral composed of silica, calcium, and titanium with few aluminum and potassium; **d** a particle of K-feldspar showing the breakdown along the cleavage that causes brightness variation; **e** inclusion composed of silica, molybdenum, and barium with minor aluminum and potassium within dissolved K-feldspar, the inclusion contains smaller inclusion of quartz; **f** altered K-feldspar particle highly affected by diagenesis. The particle shows two brightness variations where the darker tone is lower in potassium content

inclusions is those associated with most of the zirconium and heavy minerals (e.g., amphiboles and pyroxenes), while the latter includes titanium minerals (rutile) and part of molybdenum minerals.

Feldspar is the second dominant mineral within particles in both Dibdiba Formation and aeolian samples. It represents 7.6% of the total observed samples, 5.72% of which are K-feldspar while 1.9% is plagioclase. Similar to quartz particles, most of the feldspar particles were found rounded to semi-rounded in shape and free of any inclusions (Fig. 3b). Feldspars are highly susceptible to dissolution and chemical alteration commonly associated with formations of autogenic clay (particularly smectite). As a result, particles of feldspars were found

completely destroyed by dissolution under some condition forming different kinds of clay minerals. BSE image analysis shows many plagioclase (especially albite) feldspar intergrowth with K-feldspar, quartz and heavy minerals. There were mostly observed within samples mid-way between the up and downwind (Fig. 3c). Brightness variations within single feldspar particles indicate a variation in chemical composition or due to fracture or breakdown of the particle along the cleavage planes (Fig. 3d). Inclusions within feldspar containing two major elements (molybdenum and barium) were found within most of the samples. The behavior of trace elements in the feldspars under hydrothermal conditions has been studied by Liyama (1974). One of his major observations is that the solubility of barium in albite and anorthite was very small. In addition, he found that sanidine ($AlSi_3O_8$) can accommodate these elements more than albite. Molybdenum and barium were also detected within the composition of some feldspar particles (Fig. 3e). This might indicate that the feldspars were affected by diagenesis which causes the alteration of new elements within their composition. For example, barite ($BaSO_4$) was observed in quartz particles and feldspars not as inclusions but as a diagenetic product formed inside fractures and cavities (Fig. 3f).

Other particles are represented by mud particles, carbonates, and heavy minerals and all are estimated as 2.4% of the total tested samples. Mud particles dominantly contain quartz and feldspar particles (Fig. 4a). Other mud particles may contain a lot of other inclusions. The inclusions that were detected within the mud particles are mostly the same as in quartz and feldspar particles (Fig. 4b). The resolution of backscattered detectors is such that the textural details of clay minerals are intimately revealed. Furthermore, the use of energy-dispersive X-ray analysis (EDX) permits detailed quantitative geochemical and mineralogical study of different clay minerals. Owing to their fine particle size, clay minerals are recognized through whole particle analysis, through which we identify the major elements within the particle. Clay particles are dominantly containing large aggregates of quartz and feldspars. Calcrete composed of particles of calcium, mud, and quartz cemented by calcium carbonates is also observed (Fig. 4c). The carbonates within the calcrete show perfect cleavages (Fig. 4d). Heavy minerals containing inclusions are uncommon. Additionally, some exotic particles represented by a piece of glass were observed within the samples (Fig. 4e and f).

Characteristics of samples

The analysis of all samples in aeolian (downwind, mid-area, upwind) and Dibdiba Formation samples show similarities between samples with slight variations. All samples show much higher percentages of quartz and feldspar (more than 90%).

Aeolian samples

There were different types of trends observed by studying the aeolian samples. The samples were picked to be in a line traverse from up to downwind dunes. These trends are the downwind samples, upwind samples, and the mid-area samples in between. In general, the aeolian samples are similar in the major elements and minerals detected. Similarities were represented by the major elements such as titanium, zirconium, and iron that were found in a similar form in all samples. On the other hand, some differences were noticed within the variation of percentages of minor elements such as molybdenum, sulfur, and manganese that were detected in inclusions within quartz and feldspars (Table 1).

Iron, aluminum, calcium, and zirconium, respectively, are the main elements within inclusions of dune sediments. These elements were also detected in aeolian dust and aerosol particles by many researchers (Al-Dousari et al. 2019b, c). Zirconium, for example, is usually detected either with silica to form a mineral called zircon or with silica and calcium and some other times with traces of other elements such as iron, aluminum, potassium, and titanium. These two major forms of zirconium were observed all over the aeolian samples (Fig. 5a). Zircon is a common accessory mineral of igneous rock, particularly the plutonic rocks and especially in those plutonic rocks relatively rich in sodium (Fig. 5b). The mineral is frequently of use in correlating sandstones by their heavy mineral content, its distinctive feature of color, zoning, habit, or inclusions enabling the zircons of one horizon to be distinguished from those of another horizon nearby (Deer et al. 1992). The zirconium inclusions can be found separately or with other inclusions of heavy minerals within quartz particles (Fig. 5c). Zircon is a mineral that can be formed as an alteration product within quartz particles. The alterations take place through cracks or fractures within particles. As a result of such alteration, particles can be found in aeolian samples that are affected by cracks while the inclusions are not affected by the cracks that

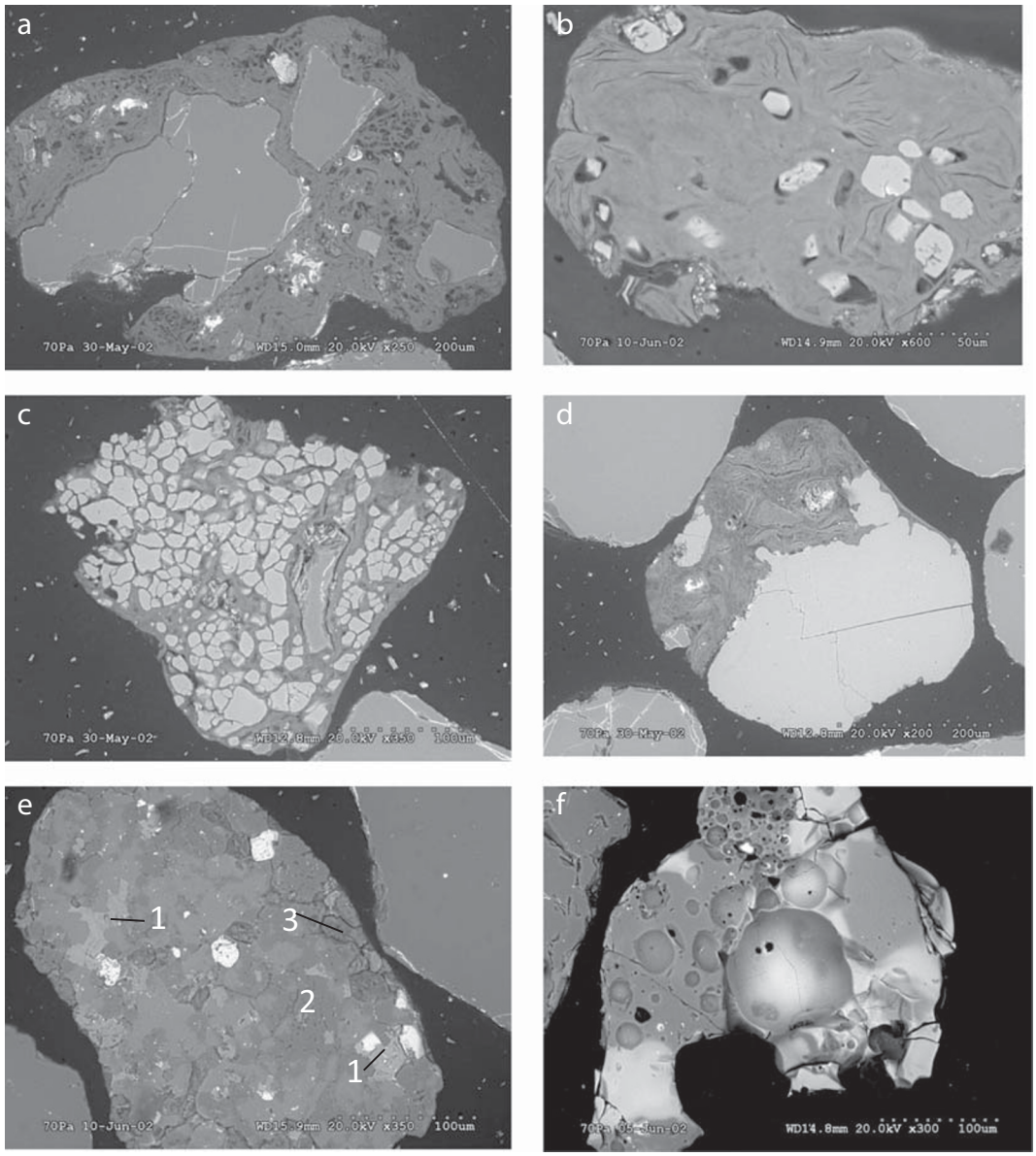

Fig. 4 Other particles represented by **a** mud particle that contains fractions of quartz; **b** another mud particle that contains several types of heavy minerals; **c** calcrete composed of carbonate particles cemented by mud; **d** particle composed of carbonate with perfect cleavages and mud with quartz fractions; **e** heavy minerals containing varieties of inclusions mica (1), zircon (2), and other heavy minerals (goethite) (3); and **f** a piece of non-pure glass found within the sediments composed mainly of silica with minor aluminum, iron, and potassium

may indicate that it forms after cracking of the particles (Fig. 5d). Altered zircon can be identified through brightness variation due to variation in element concentrations. The variations of brightness within minerals may indicate variation in chemical composition. The appearance of calcium with zirconium and silica may cause a darker tone of crystals. It has a higher brightness if the zirconium is found only with silica as zircon (Fig. 5e). Also, zircon has been detected as inclusions within the matrix composed of calcium and silica that has been inserted within cracks and fractures in quartz particles (Fig. 5f). Another example of similarities between samples can be observed within the detected titanium in aeolian samples, which are usually associated with silica and iron and sometimes with traces of aluminum, calcium, and manganese. This form of titanium mineral was

Table 1 Detection frequency for the main elements within inclusions of the aeolian and the Dibdiba Formation particles

Elements	Aeolian sample				Dibdiba Formation
	Averages (in quartz particles)				
	Average	Downwind	Mid-area	Upwind	Average
Ti	5.50	2.67	7.00	5.33	5.33
Zr	8.00	6.33	8.00	8.33	11.67
Fe	11.13	5.00	12.67	12.33	9.67
Ca	8.50	6.00	8.33	9.67	6.67
Al	11.00	4.33	12.67	13.00	10.67
Ba	2.00	1.67	2.33	2.00	2.67
Mo	1.25	0.33	1.67	1.33	3.33
S	0.38	0.00	0.67	0.33	1.67
Mn	0.50	1.00	0.00	0.67	2.33
In feldspar and other grains*					
Ti	1.63	0.33	2.33	1.67	8.33
Zr	1.25	0.33	2.33	0.67	3.33
Fe	5.00	2.33	8.00	3.33	8.67
Mo	1.00	2.33	0.67	0.67	3.00
Mn	0.63	0.67	0.67	0.67	4.00
Ba	1.13	2.33	0.67	1.00	2.33
Ca	4.00	0.67	7.33	2.67	12.67

*Other grains are clay, calcrete, heavy minerals, or intergrowth of quartz and feldspar (lithic)

noticed in most of the samples. There are seven known polymorphs of TiO_2, three of which are defined as minerals (rutile, anatase, and brookite) (Allen 1992). Rutile is common titanium mineral, and it is fairly founded as inclusions in other minerals, notably quartz, where it may take the form of long hair-like needles (Deer et al. 1992). The variation of different forms or shapes of titanium minerals that have been found in aeolian samples will be discussed later within this paper. Titanium is also commonly found as ilmenite ((Fe, Mg, Mn) TiO_3) with silica and iron and sometimes with little aluminum or calcium within both quartz and feldspar particles. Titanium occurs in six different forms within aeolian sediments. Titanium is used widely in the process equipment (heat exchangers, tanks, process vessels, valves) within military tanks and missiles (Al-Ajmi et al. 1994; Ahmed et al. 2016). The military tanks and missiles that were used during Kuwait Liberation War (1990–1991) are believed to be the main source of titanium that forms inside particle cavities and cracks. There are around 4000 military tanks were destroyed and nearly similar number of missiles were used in the war activities (Al-Dousari and Al-Hazza 2013; Ahmed and Al-Dousari 2013). Titanium forms as single separated particles and mixed particles mostly composed of titanium, iron, silica, and minor elements such as manganese or aluminum. It is characterized by brightness variation due to variation in composition (Fig. 7a). Veins of titanium mineral might be ilmenite ((Fe, Mg, Mn) TiO_3), which is common in some quartz particles (Fig. 6b). The titanium and silica with minor aluminum (anatase) are formed with lath-like crystals and were also observed within quartz particles (Fig. 6c). Smectite concentration is observed between cracks, fractures, and borders of quartz particles to form titanium minerals such as rutile (TiO_2) with needle-like or lath-like crystals (Fig. 6d). Titanium as euhedral crystals is also observed in both albite particles within aeolian samples and in Dibdiba Formation (Fig. 6e and f).

Iron is one of the most dominant elements with aluminum and zirconium in inclusions in both quartz and feldspars within all aeolian samples. Iron is usually observed in all samples with silicon and sometimes with traces of aluminum, magnesium, potassium, and titanium. Iron inclusions are commonly found in well-defined crystals, have higher brightness, and associated

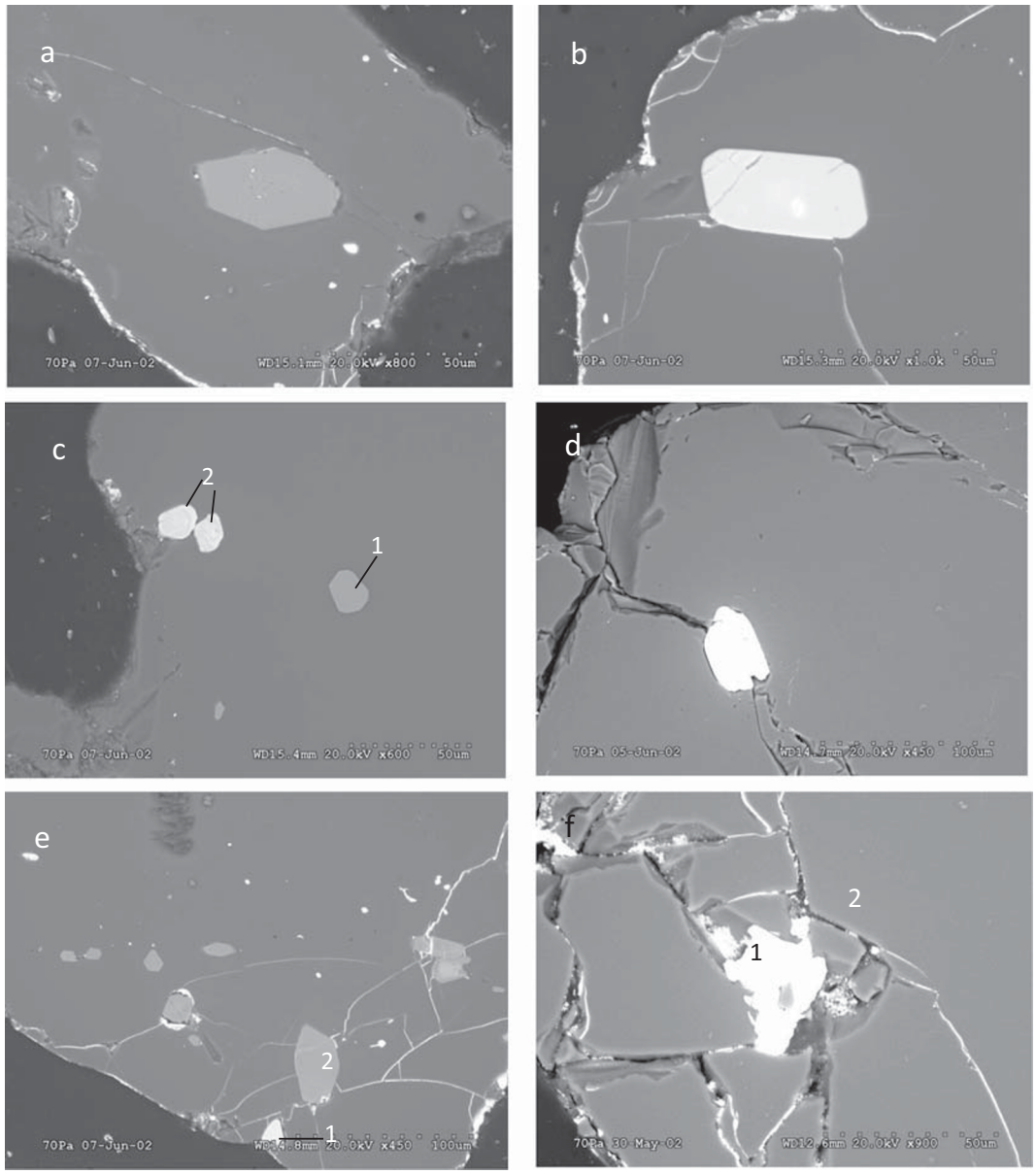

Fig. 5 Different inclusions within quartz particles **a** represented by calcium, silica, and zirconium with lower reflectance in comparison with inclusion in **b** where the silica and zirconium are two major elements **c** showing two kinds of inclusions: 1. Heavy mineral with a main content of silica, aluminum, and iron with traces of magnesium and manganese; 2. Silica and zirconium, **d** another kind of zircon formed in the way in a large fracture and not affected which indicates it is formed after as an alteration product, **e** represented single brighter inclusion zirconium wth silica (1) and dull inclusions (2) where calcium, zirconium and silica, **f** showing silica and zirconium (1) engulfed by another inclusion composed mainly by silica and calcium with little manganese (2)

with other heavy minerals, especially titanium or zirconium minerals (Fig. 7a). It is uncommon to find a matrix composed mainly of silicon, iron, and titanium with minor aluminum, but it has been observed in upwind containing varieties of other heavy mineral inclusions such as zircon, pyroxene, and hornblende (Fig. 7b). Cavities and cracks are one of the main locations that iron deposits or inclusions can be found (Fig. 7c). Iron also can be found within the composition of mica (biotite) as inclusions within quartz particles (Fig. 7d). Iron was observed as one of the major content of heavy minerals such as hypersthene (amphibole group) and covered with by small amounts of other minerals believed to be altered barium composed mainly of silicon, molybdenum, iron,

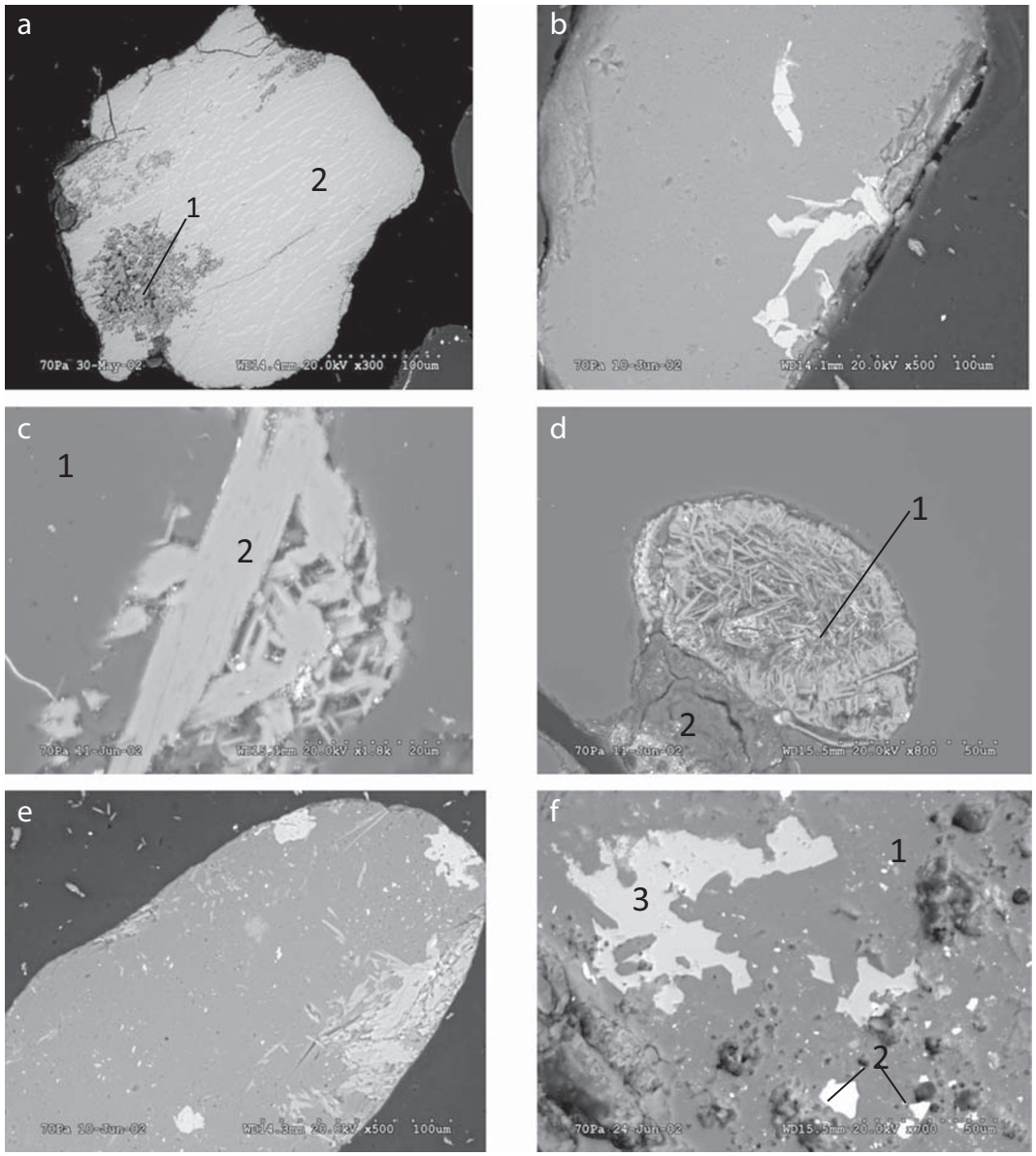

Fig. 6 Different forms of titanium mineral **a** represent a particle showing variation in brightness. The first is anatase composed of titanium, iron, silica, and lesser manganese (1) and the darker tone contains more iron, more than titanium without manganese (2); **b** veins of silica, calcium, titanium, and aluminum (ilmenite) within quartz particle; **c** lath-like crystals of anatase (1) composed of titanium and silica with minor aluminum within quartz particle (2); **d** rutile (1) formed due to alteration from smectite (2) in the border of quartz particle; **e** albite particle (1) contains inclusions of ilmenite (2) and epidote (3); and **f** euhedral crystals within the quartz particle in the sample from the Dibdiba Formation

calcium, and barium (Fig. 7e). Garnet (almandine) is more commonly found within groups of inclusions in single particles of quartz or feldspar (Fig. 7f).

Barium is found in many feldspars and quartz and always associated with molybdenum or sulfur. Barium is also detected within most of the samples in the composition of the feldspar. Barium is found within the molybdenum as mineral inclusions, and with sulfur as an alteration product in barite ($BaSO_4$). Barite was detected within quartz particles in downwind, mid-area, and upwind samples. The appearance of barium in the composition of feldspars indicates early diagenesis and may give a good sign that the feldspar is of a sedimentary origin.

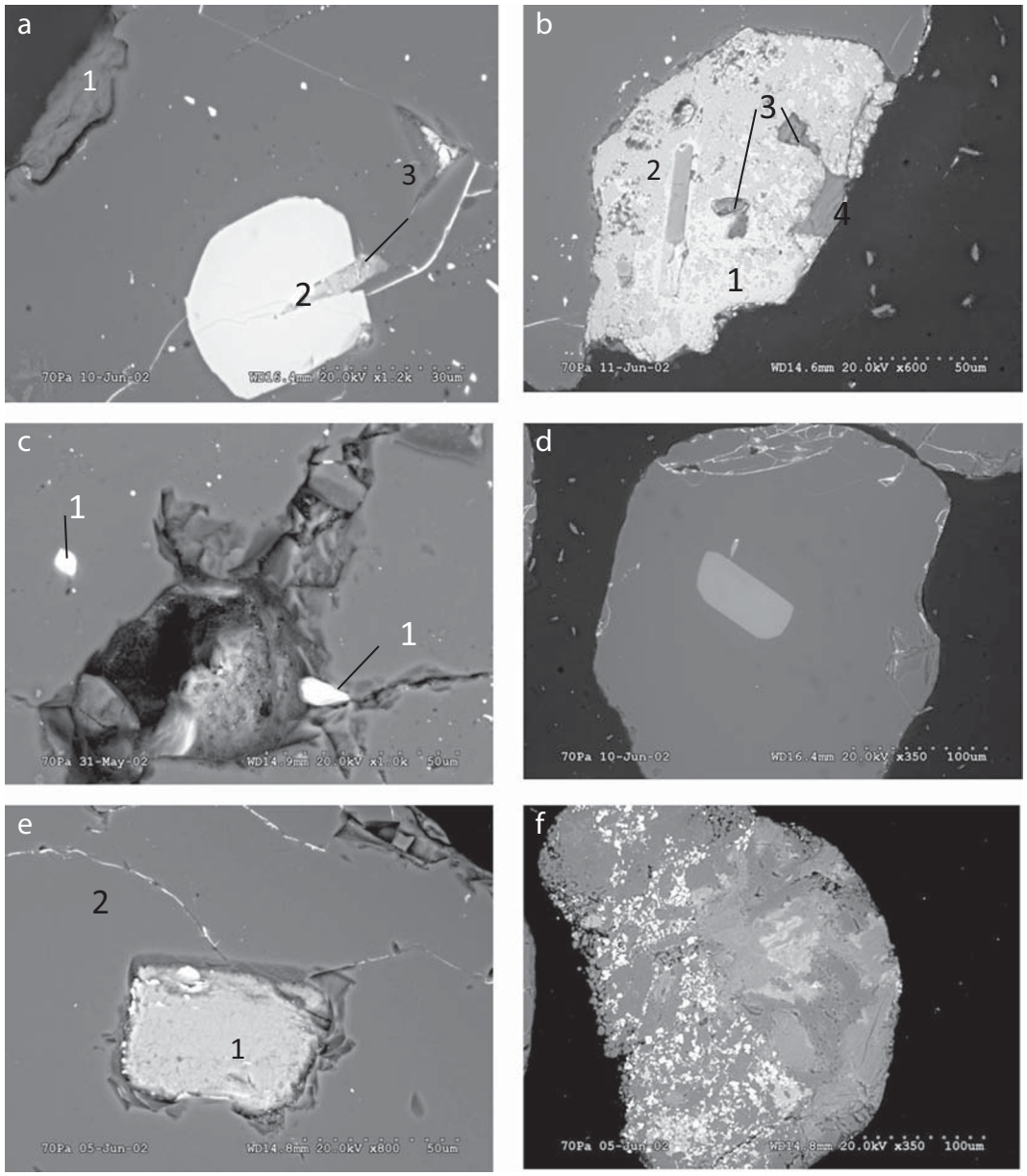

Fig. 7 Several particles of Aeolian sample containing heavy minerals. **a** Smectite are at the border of quartz particle (1), higher brightness inclusion composed of silica and iron (2) engulfing another one (sphene) (3); **b** a matrix composed of iron, silica, titanium, and traces of aluminum (1) containing a variety of inclusions, silica, calcium, zircon, and titanium (2), pyroxene (3), and hornblende with altered titanium (4); **c** zircon (1) inserted into a cavity coated by silica, magnesium, and iron (2); **d** biotite mica as large inclusion within a quartz particle; **e** hypersthene inclusion (1) containing small inclusion composed of silica, molybdenum, iron, calcium, and barium; and **f** a feldspar particle full of inclusions of garnet minerals (almandite)

Generally, lower inclusion counts were noted within quartz and feldspars in the downwind samples in comparison with other samples. The differences are found in the existence and the frequency of detection of certain elements within one group of samples compared with another. Silicon, aluminum, potassium, and calcium were all detected in all aeolian samples except in downwind samples. Potassium and calcium are never found in any of the inclusions within feldspars in downwind samples. The aluminum percentages gradually increase upwind. Sodium appears more within the inclusions of the area in between the up and downwind samples.

Table 2 Percentages and averages of major elements detected in inclusions within quartz and feldspars of the aeolian and the Dibdiba Formation samples

Elements	Aeolian sample				Dibdiba Formation
	Averages (in quartz particles)				
	Average	Downwind	Mid-area	Upwind	Average
Ti	9.7	8.9	9.8	9.3	10.0
Zr	18.4	25.1	15.1	17.7	21.0
Fe	22.7	16.3	24.1	22.2	17.4
Ca	18.5	22.3	16.7	19.2	13.2
Al	21.4	14.2	23.3	24.1	20.4
Ba	4.8	8.1	5.9	3.4	4.7
Mo	2.7	0.8	3.9	2.6	6.1
S	0.6	0.0	1.1	0.5	3.1
Mn	1.2	4.4	0.0	1.1	4.2
Incl no.+	48.3	27.3	53.3	53.0	54.0
In feldspar and other grains*					
Ti	9.9	2.4	12.0	11.9	19.0
Zr	6.7	2.4	10.3	5.3	8.2
Fe	33.9	22.7	37.9	33.8	21.4
Mo	7.8	26.3	1.9	5.3	7.5
Mn	7.4	10.8	4.5	8.6	8.1
Ba	9.0	26.3	1.9	8.3	5.7
Ca	25.3	9.0	31.7	26.9	30.2
Incl no.+	14.6	9.0	22.0	10.7	42.3

*Other grains are clay, calcrete, heavy minerals, or intergrowth of quartz and feldspar

+Average number of inclusions detected

Moreover, it has never been detected within the downwind samples. Barium is an element is not detected within any of the feldspar inclusions within the mid-area samples. There was no trace of barium observed in upwind samples either in quartz or in feldspar inclusions. The average percentages of detected barium within inclusions in quartz and feldspar show gradual increases downwind (Table 2).

Titanium, zirconium, and iron are the three major elements that are found in inclusions within quartz particles in all samples, but it varies in the percentages from one sample to another. Titanium and iron, for example, are little lower within inclusions of quartz and feldspars downwind compared with upwind. On the other hand, zirconium is present in higher percentages within inclusions of quartz particles in downwind compared with mid-area and upwind, but lower in feldspars.

Molybdenum, sulfur, and manganese are three minor elements detected in inclusions within quartz and feldspar particles in a few samples. Molybdenum is found in lower percentages within inclusions of quartz particles in downwind but higher within feldspars due to a small total number of detected inclusions in feldspars. Sulfur is only found with barium as barite. It has been detected in three samples in the mid-area and the upwind. Manganese is found as a minor component and always associated with iron and it is more detected downwind.

The Dibdiba formation samples

Duricrusts are secondary superficial deposits that form a hard crust of different composition, that originated by the chemical precipitation of minerogenous matter in free surfaces or within pores of the primary sediments. They are found extensively in the Dibdiba Formation

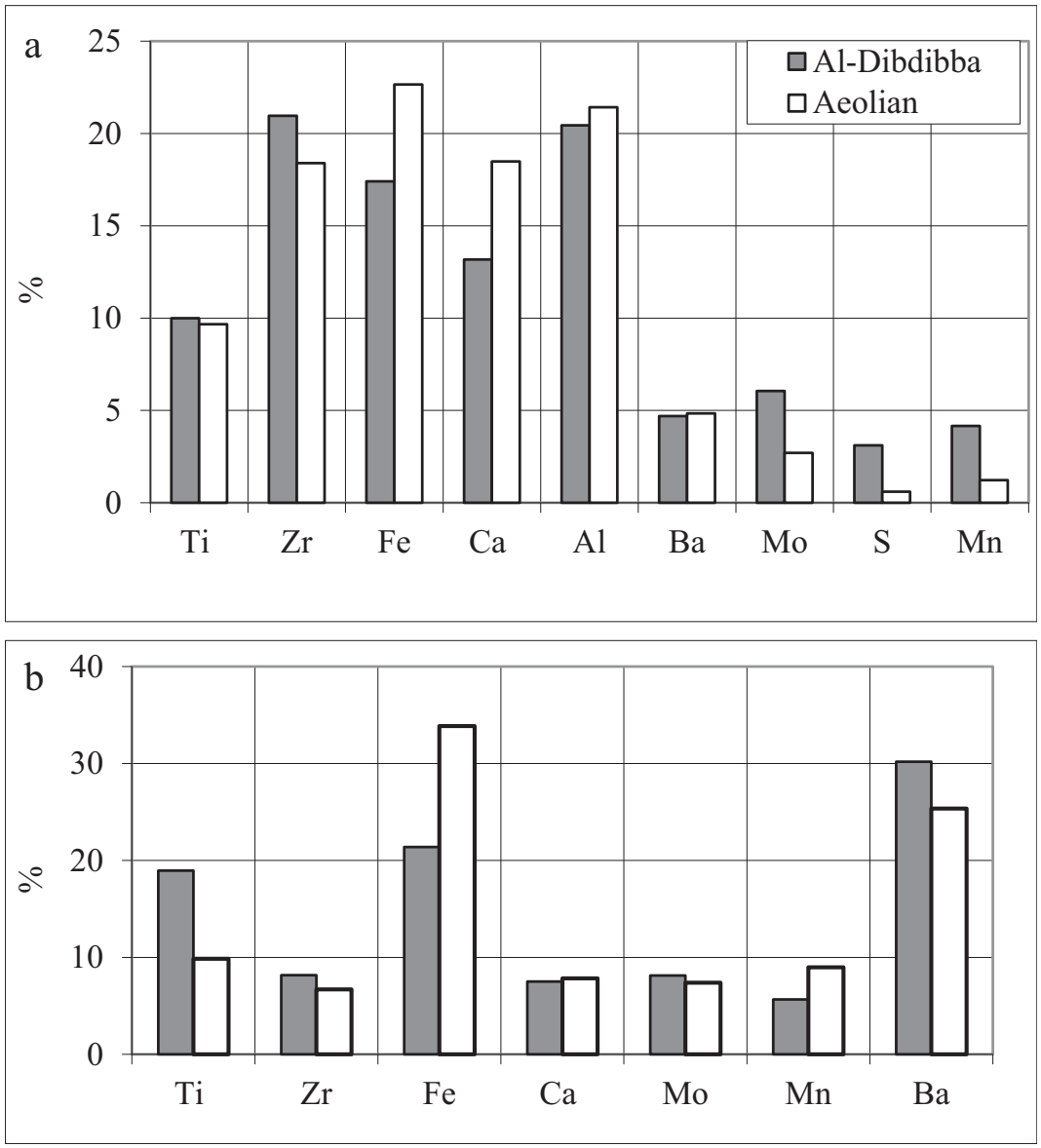

Fig. 8 Histogram showing variations in percentages of detected elements within quartz (**a**) and feldspar (**b**) inclusions

(Khalaf et al. 1994). Although the main matrix is carbonate, some clay minerals may be present in the matrix. The clay matrix (especially smectite) acts as a cementation matrix within Dibdiba Formation. Duricrust (calcrete or gypcrete) may contain a variety of elements such as titanium. Through natural solubility, the smectite may concentrate between cracks, fractures, and borders of quartz particles to form titanium minerals such as rutile (TiO_2) with needle-like or lath-like crystals. Titanium crystals are normally formed inside small cavities or fractures within quartz particles. These kinds of quartz particles were found in several samples within both groups (aeolian and Dibdiba Formation samples) that might indicate that the aeolian samples may come mainly from Dibdiba Formation.

The Dibdiba Formation shows uniformity between the three samples, especially in the major elements. The variations between samples are very limited. There are many similarities between the aeolian and Dibdiba Formation samples (Fig. 8 a and b). The close similarities are dominantly noticed within the major elements (titanium, zirconium, and iron). Variations between the two

groups of samples are observed in the minor elements (molybdenum, sulfur, and manganese).

The titanium average percentage in inclusions of quartz is 10% for both aeolian and Dibdiba Formation samples. The two groups of samples have nearly the same percentage in detected aluminum. Aeolian samples show slightly higher iron and calcium in inclusions within quartz and feldspar. The iron and calcium are 22.7 ± 7% and 18.5 ± 4%, respectively, in aeolian samples in quartz inclusions, while it is only 17.4 ± 6% and 13.2 ± 7%, respectively, in Dibdiba Formation samples. Zirconium is a little higher in Dibdiba Formation samples (21 ± 6%) than the aeolian samples (18.4 ± 7%).

Barium in all Dibdiba Formation samples is commonly found in feldspars and quartz and is always associated with molybdenum or sulfur. No further changes were noticed during the comparison between the barium inclusions within quartz in both Dibdiba Formation (4.7%) and the aeolian (4.8%) samples. Only a slight change in the percentages of barium was observed within inclusions in feldspars in both the Dibdiba Formation (6 ± 3%) and the aeolian (9 ± 12%) samples.

Characteristics of detected elements

There are eleven major and sub-major elements studied separately in relation to other elements. These elements, respectively, are aluminum (Al), potassium (K), calcium (Ca), sodium (Na), barium (Ba), titanium (Ti), iron (Fe), zirconium (Zr), molybdenum (Mo), magnesium (Mg), and manganese (Mn).

Conclusion

The inclusions can give a good indication of the provenance of the particles. Analysis of aeolian and Dibdiba Formation sediment samples using backscattered electron microscopy shows that quartz represents 89.9% as an average for all tested samples. The content of inclusions within quartz, feldspars, and other minerals can be used as a fingerprint for aeolian sediments. The nine aeolian samples were chosen from a line transect across the main wind corridor, representing the downwind, mid, and upwind areas (three in each set). There are many similarities between the aeolian and Dibdiba Formation samples. The Dibdiba Formation shows uniformity between the three samples, especially in the major elements. The variations between samples are very limited. Titanium, for example, through natural solubility in smectite, may be concentrated in cracks, fractures, or borders of quartz particles to form rutile (TiO_2) with needle-like or lath-like crystals. Titanium is also found in other forms of minerals within the two groups of sediments, which may indicate close similarities between the two groups. Also, no further changes were noticed during the comparison between the barium inclusions within quartz that are found in both the Dibdiba Formation (4.7%) and the aeolian (4.8%) samples. The military missiles and tanks that were used during Kuwait Liberation War (1990–1991) are believed to be the main source of secondary titanium that forms inside particle within borders cracks and cavities. Barium was found into two kinds of mineral components; the first in barite as a diagenesis product, while the second is as primary inclusions. Both forms were also observed within the aeolian and the Dibdiba Formation samples. It is concluded that the content of inclusions within quartz, feldspars, and other minerals can be used as a fingerprint for aeolian sediments. Therefore, future studies will concentrate on regional variations with dunes upwind in Iraq and downwind in Saudi Arabia.

Compliance with ethical standards

Conflict of interest The authors declare that they have no conflict of interest.

References

Aba A, Al-Dousari AM, Ismaeel A (2018) Atmospheric deposition fluxes of 137Cs associated with dust fallout in the northeastern Arabian Gulf. J Environ Radioact 192:565–572. https://doi.org/10.1016/j.jenvrad.2018.05.010

Aba A, Al-Dousari AM, Ismael A (2016) Depositional characteristics of 7Be and 210Pb in Kuwaiti dust. J Radioanal Nucl Ch 307:15–23. https://doi.org/10.1007/s10967-015-4129-y

Ahmed M, Al-Dousari AM (2013) Geomorphological characteristics of the Um-Rimam depression in northern Kuwait. Kuwait J Sci 40(1):165–178

Ahmed M, Al-Dousari N, Al-Dousari AM (2016) The role of dominant perennial native plant species in controlling the mobile sand encroachment and fallen dust problem in Kuwait. Arab J Geosci 9(2):134. https://doi.org/10.1007/s12517-015-2216-6

Abd El-Wahab RH, Al-Rashed AR, Al-Dousari A (2018) Influences of physiographic factors, vegetation patterns and human impacts on aeolian landforms in arid environment.

Arid Ecosyst 8(2):97–110. https://doi.org/10.1134/S2079096118020026

Al-Ajmi D, Misak R, Khalaf FI, Al-Sudairawi M, Al-Dousari AM (1994) Damage assessment of the desert and coastal environment of Kuwait by remote sensing (VT001C). Report no. KISR 4405. Kuwait Institute for Scientific Research, Kuwait

Al-Awadhi JM, Al-Dousari A, Al-Enezi A (2000) Barchan dunes in northern Kuwait. Arab Gulf J Sci Res 18(1):32–40

Al-Dousari AM, Alsaleh A, Ahmed M, Misak R, Al-Dousari N, Al-Shatti F, Elrawi M, William T (2019a) Off-road vehicle tracks and grazing points in relation to soil compaction and land degradation. Earth Syst Environ 3(3):471–482. https://doi.org/10.1007/s41748-019-00115-y

Al-Dousari A, Al-Nassar W, Al-Hemoud A, Alsaleh A, Ramadan A, Al-Dousari N, Ahmed M (2019b) Solar and wind energy: challenges and solutions in desert regions. Energy 176:184–194. https://doi.org/10.1016/j.energy.2019.03.180

Al-Dousari AM, Ahmed M, Al-Dousari N, Al-Awadhi S (2019c) Environmental and economic importance of native plants and green belts in controlling mobile sand and dust hazards. Int J Environ Sci Technol 16:2415–2426. https://doi.org/10.1007/s13762-018-1879-4

Al-Dousari AM, Aba A, Al-Awadhi S, Ahmed M, Al-Dousari N (2016) Temporal and spatial assessment of pollen, radionuclides, minerals and trace elements in posited dust within Kuwait. Arab J Geosci. https://doi.org/10.1007/s12517-015-2182-z

Al-Dousari AM, Al-Hazza A (2013) Physical properties of aeolian sediments within major dune corridor in Kuwait. Arab J Geosci 6(2):519–527. https://doi.org/10.1007/s12517-011-0353-0

Al Enezi E, Al-Dousari A, Al-Shammeri F (2014) Modeling adsorption of inorganic phosphorous on dust fallout in Kuwait. J Eng Res 2(2):1–14

Allen F (1992) Mineral definition by HRTEM: problems and opportunities. In: Buseck PR (ed) Minerals and reactions atomic scale: transmission electron microscopy, vol 8, pp 289–333

Chalcraft D, Pye K (1984) Humid tropical weathering of quartzite in southeastern Venezuela. Z Geomorphol 28:321–332

Deer WA, Howie RA, Zussman J (1992) An introduction to the rock-forming minerals. 2nd edn. Longman. Essex

Khalaf FI, Al-Ajmi D, Al-Dousari A (1994) Detrital palygorskite in recent terrestrial and marine sediments of Kuwait. Egypt J Geol 38(2):537–554

Krinsley D, Pye K, Boggs S, Tovey NK (1998) Backscattered scanning electron microscopy and image analysis of sediments and sedimentary rocks. Cambridge University Press, Cambridge

Liyama JT (1974) Behaviour of trace elements in feldspars under hydrothermal conditions. In: Mackenzie WE, Zussman J (eds) The feldspars, vol 4, pp 552–573

Malathy P, Vignesh K, Rajarajan M, Suganthi A (2014) Enhanced photocatalytic performance of transition metal doped Bi $_2O_3$ nanoparticles under visible light irradiation. Ceram Int *40*(1 PART A):101–107

Reed SJ, Ware NG (1975) Quantitative electron microprobe analysis of silicates using energy-dispersive X-ray spectrometry. J Petrol 16(1):499–519

Sudha M, Senthilkumar S, Hariharan R, Suganthi A, Rajarajan M (2012) Synthesis, characterization and study of photocatalytic activity of surface modified ZnO nanoparticles by PEG capping. J Sol-Gel Sci Technol 65:301–310

Vignesh K, Priyanka R, Rajarajan M, Suganthi A (2013) Photoreduction of Cr (VI) in water using Bi_2O_3–ZrO_2 nanocomposite under visible light irradiation. Mater Sci Eng B 178(2):149–157